Catalytic Site Nucleotide Binding and Hydrolysis in F_1F_o-ATP Synthase†

Sabine Löbau, Joachim Weber, and Alan E. Senior*

Department of Biochemistry and Biophysics, Box 712, University of Rochester Medical Center, Rochester, New York 14642

Received March 30, 1998; Revised Manuscript Received June 2, 1998

ABSTRACT: F_1F_o-ATP synthase was purified from *Escherichia coli* βY331W mutant. The β-Trp-331 provided a specific fluorescent probe of catalytic site nucleotide binding. Physiological (mM) concentration of substrate MgATP filled all three catalytic sites. With MgATP or MgADP the catalytic sites showed marked binding cooperativity and asymmetry, which was dependent on Mg^{2+}. Nucleotide binding was fast, with $k_{on} = \sim 6 \times 10^5\ M^{-1}\ s^{-1}$. P_i at physiological concentration (5 mM) did not bind to catalytic sites. Measurement of MgATP hydrolysis and binding under identical conditions as a function of MgATP concentration revealed that V_{max} was achieved only when all three catalytic sites were filled in every enzyme molecule. The enzyme species with two catalytic sites occupied and one site empty displayed low, nonphysiological catalytic rate. This is the first characterization of nucleotide binding parameters in F_1F_o. The fact that the behavior of purified F_1F_o was similar in most respects to that of isolated F_1 demonstrated that the presence of the additional F_o subunits *a*, *b*, and *c*, and also fixed stoichiometric amounts of ϵ and δ, does not affect catalytic site properties. The results impact on possible catalytic mechanisms, namely, they emphasize that P_i cannot simply bind spontaneously, that an enzyme species with all three sites occupied is the only catalytically competent species, and that release of product and binding of substrate cannot be simultaneous, rather the former must precede the latter.

In *Escherichia coli* the membrane-bound F_1F_o-ATP synthase catalyzes ATP-driven proton extrusion across the plasma membrane, or proton-gradient-driven ATP synthesis in the terminal step of oxidative phosphorylation, depending on the metabolic conditions. The enzyme consists of eight subunits and is readily separable into the F_1 sector (five subunits, $\alpha_3\beta_3\gamma\delta\epsilon$) and the F_o sector (three subunits, ab_2c_{10-12}). The three catalytic ATP hydrolysis and synthesis sites are located on the F_1 sector, primarily on the β-subunits, and the F_o sector provides the proton conduction path through the membrane (for recent reviews, see refs *1*, *2*). Important recent advances have come from X-ray structural elucidation of a major part of the F_1 sector of mitochondrial enzyme (*3*−*5*), the $\alpha_3\beta_3$ complex of the enzyme from the thermophilic *Bacillus* PS3 (6), and the isolated *E. coli* subunit ϵ (*7*). NMR studies of isolated *E. coli* subunits ϵ and δ (*8*, *9*) and subunit *c* (*10*) have added to this impressive list of structure information. Furthermore, functional concepts have been advanced by the experimental demonstration, in the $\alpha_3\beta_3\gamma$ complex of *Bacillus* PS3, that ATP hydrolysis drives rotation of the γ-subunit within the $\alpha_3\beta_3$ hexagon (*11*, *12*), confirming that the three catalytic sites act in a sequential manner during steady-state catalysis (*13*).

To understand the mechanism of ATP-driven proton pumping and ATP synthesis, it is necessary to define the functional characteristics and behavior of the catalytic sites in detail. For this purpose the technique of site-directed tryptophan fluorescence has proved valuable. Introduction of Trp residues in the catalytic sites at residue β-Tyr-331 or at residue β-Phe-148 allowed direct and specific measurement, in purified *E. coli* F_1, of occupancy of catalytic sites by substrates MgADP or MgATP during steady-state ATP hydrolysis (*18*, *19*).[1] The Trp fluorescence signals also allowed determination of catalytic site binding affinity for a wide range of substrates and substrate analogues under true equilibrium conditions (*20*−*22*). This work established that the three catalytic sites are asymmetric when they bind the natural substrate MgATP, that only the enzyme species with all three catalytic sites filled with nucleotide is catalytically competent (i.e., capable of carrying out steady-state catalysis at physiologically necessary rates), that at normal cellular concentrations of nucleotide the enzyme species with all three catalytic sites filled is easily the predominant form, and that the crucial determinant of catalytic site asymmetry is coordination of the Mg^{2+} moiety of substrates MgATP or MgADP.

As with the vast majority of previous enzymological studies of ATP synthase, the above Trp fluorescence work used isolated F_1 as the experimental material. With a growing body of evidence showing that F_1F_o acts as a concerted molecular motor, it is important to investigate and establish properties of the catalytic sites in the intact, eight-subunit complex, about which little has so far been reported. For this purpose the Trp fluorescence approach appeared suitable and we chose initially to use the β-Trp-331 probe because of its large signal. In this paper we have purified

† Supported by NIH Grant GM25349 to A.E.S. and by Deutsche Forschungsgemeinschaft Grant Lo 656/1-1 to S.L.

* Author to whom correspondence should be addressed.

[1] Parallel studies have been published using the Trp probe α-Arg-365 → Trp, situated in noncatalytic nucleotide sites. This allowed extensive characterization of nucleotide binding parameters of noncatalytic sites (*14*−*17*). It is evident that the noncatalytic and catalytic sites show distinctly different properties and that the Trp probes are specific for the respective sites.

S0006-2960(98)00715-6 CCC: $15.00
Published on Web 07/09/1998

F_1F_o from *E. coli* βY331W mutant, demonstrated its functional and structural integrity, and characterized the catalytic sites in terms of substrate binding characteristics and occupancy during steady-state ATP hydrolysis.

EXPERIMENTAL PROCEDURES

Materials. Phosphatidylcholine (PC)[2] from egg yolk and distearoyl-phosphatidylglycerol (PG) were purchased from Avanti Polar Lipids; asolectin and luciferin/luciferase reagent (L0633) were obtained from Sigma, and ADP (monopotassium salt) was from Boehringer Mannheim.

Enzyme Preparation. E. coli F_1F_o was purified according to Moriyama et al. (*23*) with the following minor modifications. Cells were grown in minimal medium with supplements and 30 mM glucose to late logarithmic phase, harvested by centrifugation, resuspended, and disrupted by passage of the cell suspension twice through a French press. Purification of plasma membranes was achieved by sucrose gradient centrifugation (*23*). The membranes were extracted with 0.8% (w/v) *n*-octyl-β-D-glucopyranoside (OG), centrifuged, then the pellet was re-extracted with 2% (w/v) OG; the final supernatant containing F_1F_o was loaded on linear glycerol gradients (10−25% v/v) and centrifuged for 18 h at 26 000 rpm in an SW28 rotor. Fractions were assayed for ATPase activity and protein, and peak fractions were pooled and stored as aliquots at −70 °C. The profiles of the glycerol gradients were the same as previously reported (*23*). Wild-type F_1F_o was isolated from strain SWM1 (*24*), and βY331W mutant F_1F_o from strain pSWM4/JP17 (*18*).

Reconstitution of F_1F_o in Proteoliposomes for ATP-Driven Proton Pumping Experiments. F_1F_o was added to purified asolectin (*25*) at a ratio of 1/125 (w/w). The lipid was previously thoroughly dried, and the protein (0.25 mg/mL) was added in 1% (w/v) OG. The mixture was vortexed and clarified in a sonication bath at 4 °C. After incubation on ice for 20 min the mixture was diluted 30-fold in 10 mM HEPES, pH 7.5, and stirred for 10 min at room temperature. Proteoliposomes were collected by centrifugation, resuspended in 10 mM HEPES buffer (0.25 mg of protein/mL), and either used immediately or stored at −70 °C.

Measurement of ATP-Driven pH Gradient Formation. Asolectin proteoliposomes prepared as above (50 μL) were added to buffer (10 mM HEPES, 5 mM $MgSO_4$, 100 mM KCl, pH 7.5) containing 2.5 μM 9-amino-6-chloro-2-methoxyacridine (ACMA) in a 2 mL stirred volume. The reaction was initiated by addition of 2 mM ATP. Subsequently, valinomycin (1 μM) and carbonyl cyanide *m*-chlorophenylhydrazone (CCCP) (5 μM) were added as indicated. Fluorescence quenching was monitored at room temperature in an SLM Aminco-Bowman Series 2 fluorometer with $\lambda_{exc} = 410$ nm and $\lambda_{em} = 480$ nm.

Reconstitution of F_1F_o in Proteoliposomes for ATP Synthesis Experiments. F_1F_o was reconstituted into preformed liposomes which were prepared as follows. PC and PG were mixed at a ratio of 80/20 (w/w), thoroughly dried, and solubilized in buffer containing 20 mM Tricine, 20 mM succinate, 0.6 mM KCl, 80 mM NaCl, pH 8.0, 3% (w/v) OG. After dialysis at room temperature against a 1000-fold volume of the same buffer without OG, liposomes were passed consecutively through 0.4 μm and 0.2 μm polycarbonate filters. Reconstitution of F_1F_o was achieved by detergent removal with polystyrene beads (BioRad) (*26*), following the protocol of Fischer et al. (*27*).

Measurement of ATP Synthesis. ATP synthesis assays were performed as described by Fischer et al. (*27*). Briefly, 43 μL of PC/PG proteoliposomes containing wild-type or βY331W mutant F_1F_o were preincubated for 2 min at room temperature in 217 μL of buffer containing 20 mM succinate, pH 4.7, 0.6 mM KCl, 2.5 mM $MgCl_2$, 5 mM NaH_2PO_4, 0.2 mM ADP, and 8 μM valinomycin. This suspension was then injected into 240 μL of buffer (200 mM Tricine, pH 8.8, 50 mM KCl, 2.5 mM $MgCl_2$, 5 mM NaH_2PO_4, 0.2 mM ADP, and 1.6 mg/mL of luciferin/luciferase reagent). ATP synthesis was measured at room temperature and recorded in a luminometer TD-20/20 (Turner Designs) in the data flow mode, registering data points every 0.2 s. Signals were calibrated by adding 100 pmol of authentic ATP. For calculation of ATP synthesis rates we assumed a molecular weight of $F_1F_o = 535$ kDa, that all F_1F_o added is reconstituted, and that all F_1F_o molecules are reconstituted with F_1 facing out.

ATPase Assays. Specific ATPase activities were measured in 50 mM Tris/H_2SO_4, 10 mM ATP, 4 mM $MgSO_4$, pH 8.5, at 30 °C. Dependence of enzymatic activity on substrate concentration was measured at 23 °C in buffer containing 50 mM Tris/H_2SO_4, pH 8.0, with varying concentrations of ATP (0.02−10.0 mM) and $MgSO_4$ (0.008−4.0 mM) in a constant ratio of 2.5/1. Released P_i was determined by colorimetric assays (*28*, *29*). K_M and V_{max} (k_{cat}) values were calculated by nonlinear regression analysis, assuming simple Michaelis−Menten kinetics (one K_M value).

Analysis of Endogenous F_1F_o-Bound ATP and ADP. For denaturation, F_1F_o samples were added rapidly to a 25-fold volume of assay buffer (60 mM glycine, pH 7.75, 10 mM $MgCl_2$, 1 mM KCl, 1.5 mM EDTA, 2.5 mM 2-mercaptoethanol) at 100 °C and boiled for 3 min, then cooled on ice and centrifuged. ATP and ADP contents were analyzed by the luciferin/luciferase method. For ATP analysis the sample volume was made up to 1 mL with assay buffer. To start the reaction, luciferin/luciferase reagent was added to 0.4 mg/mL. After exactly 30 s, light emission was measured in a Beckman LS17000 liquid scintillation counter. For ADP analysis 20 μL of 70 mM glycine, pH 7.75, 9 mM $MgCl_2$, 5 mM KCl, 2 mM EDTA, 2 mM phosphoenolpyruvate, and 500 units/mL of pyruvate kinase were added to 180 μL of denatured sample, and the mixture was incubated for 40 min at room temperature. Light emission was measured upon addition to 1 mL of assay buffer containing 0.4 mg/mL of luciferin/luciferase reagent, and total ATP was determined. ATP and ADP recoveries were close to 100%, as judged by the method of additions using authentic ATP and ADP.

Tryptophan Fluorescence Measurements. The procedures followed those previously described (*30*). Final enzyme concentration in the cuvette was 20−25 nM. Analysis of binding of MgATP, MgADP, and ATP was performed as described (*30*). Inner filter effects were controlled by running parallel experiments with wild-type enzyme (which showed no fluorescence change on addition of nucleotide). MgATP and MgADP concentrations were calculated assuming K_d

[2] Abbreviations: OG, *n*-octyl-β-D-glucopyranoside; ACMA, 9-amino-6-chloro-2-methoxyacridine; PC, phosphatidylcholine; PG, phosphatidylglycerol; CCCP, carbonyl cyanide *m*-chlorophenylhydrazone; DCCD, dicyclohexylcarbodiimide.

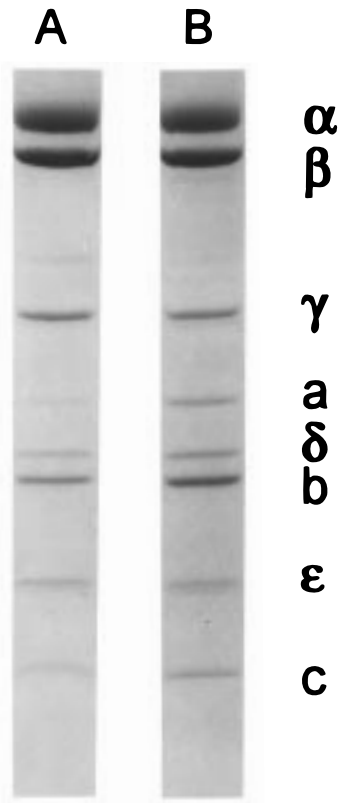

FIGURE 1: Properties of wild-type and βY331W mutant purified F_1F_o. SDS−polyacrylamide gel electrophoresis of F_1F_o. Wild-type F_1F_o (16 μg, lane A) and βY331W F_1F_o (16 μg, lane B) were separated on a 13% SDS-gel according to (*33*) and stained with Coomassie Brilliant Blue R. The eight component subunits are labeled.

values of 20 μM and 78 μM for MgATP and MgADP complexes (*31*). For measurements of nucleotide binding in the presence of phosphate, 5 mM NaP_i, pH 8.0, was added before the addition of nucleotide.

Routine Procedures. Protein was estimated as in (*32*), and SDS-gel electrophoresis as in (*33*), using 13% gels.

RESULTS

Properties of Purified Wild-Type and βY331W Mutant F_1F_o Enzymes. Wild-type and βY331W mutant F_1F_o enzymes were purified according to the method of Moriyama et al. (*23*). We changed the conditions slightly so that the glycerol gradient used to separate F_1F_o from other OG-solubilized proteins was a 10−25% gradient, giving better separation than achieved by the 10−30% gradient of the original protocol. Protein and ATP hydrolysis profiles from glycerol gradients were comparable to (*23*). Added pure F_1 ran well in front of F_1F_o on the glycerol gradient in a test experiment, and no evidence for separation of F_1 from F_o was seen during the F_1F_o preparations. Yields were in the range of 0.2 to 0.4 mg of purified F_1F_o per gram of wet cells for both wild-type and βY331W. Both clearly showed all eight subunits and few impurities in SDS-gels (Figure 1). Specific ATPase activity (30 °C, pH 8.5) for the βY331W mutant F_1F_o was 12.2 U/mg, which was about half that of wild-type enzyme (23.2 U/mg), consistent with results reported for the respective F_1 enzymes (*18*). K_M(MgATP) for βY331W F_1F_o was 24 μM, whereas wild-type enzyme showed a higher K_M(MgATP) of 140 μM. Thus, k_{cat}/K_M was

Table 1: Bound ATP and ADP in Purified F_1F_o Preparations Assayed by the Luciferin/Luciferase Method[a]

F_1F_o	ATP (mol/mol)	ADP (mol/mol)
wild-type	1.54 ± 0.10	0.01 ± 0.10
βY331W	1.42 ± 0.30	0.01 ± 0.12

[a] All data are given as average ± standard deviation, based on quadruplicate experiments.

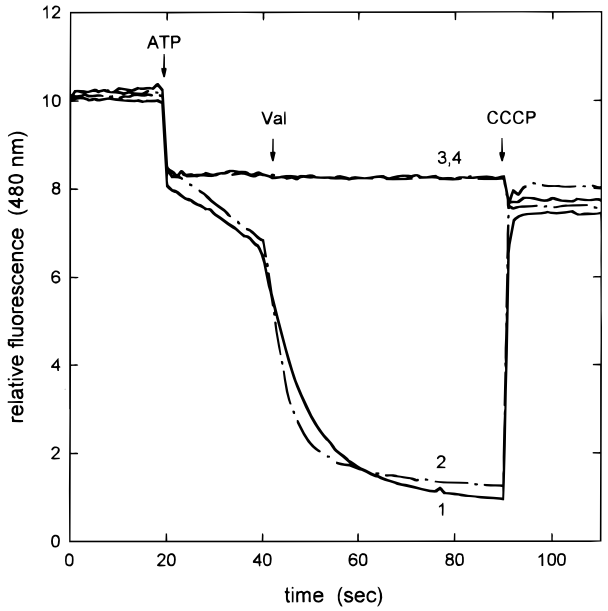

FIGURE 2: Properties of wild-type and βY331W mutant purified F_1F_o. ATP-driven proton pumping in proteoliposomes. F_1F_o was reconstituted into asolectin vesicles and pH gradient formation was assayed by ACMA fluorescence quenching as described in Experimental Procedures. The additions shown are ATP (2 mM), valinomycin (1 μM), and CCCP (5 μM). Traces 1 and 3, wild-type F_1F_o; traces 2 and 4, βY331W F_1F_o; traces 1 and 2, no DCCD; traces 3 and 4 were measured after preincubation of F_1F_o in 150 μM DCCD for 20 min at room temperature prior to reconstitution.

4.6×10^6 M^{-1} s^{-1} for βY331W F_1F_o and 1.5×10^6 M^{-1} s^{-1} for wild-type F_1F_o, in good agreement with data on F_1 (*18*). To determine the occupancy of the nucleotide binding sites by endogenous nucleotide in preparations of purified F_1F_o, the amount of ATP and ADP was measured in denatured enzyme using the luciferin/luciferase method. These results are shown in Table 1. For wild-type F_1F_o a total content of 1.54 mol of nucleotide (ATP plus ADP) per mol of enzyme was detected, for βY331W it was 1.42 mol/mol of F_1F_o. Virtually all of the bound nucleotide was ATP, and essentially none was ADP. Since the F_1F_o is purified in buffers containing 0.5−2.0 mM $MgCl_2$, without any added nucleotide, and the bound ATP survived the purification, this indicated that the bound nucleotide was in noncatalytic sites and the catalytic sites were empty.

ATP-Driven Proton Pumping by Purified F_1F_o in Reconstituted Proteoliposomes. To further investigate properties of wild-type and βY331W F_1F_o, both enzymes were reconstituted into asolectin proteoliposomes and tested for their ability to perform ATP-driven proton pumping as measured by ACMA fluorescence quenching. Upon addition of 2 mM ATP to the proteoliposomes, a rapid decrease in fluorescence occurred which was accelerated by adding 1 μM valinomycin (Figure 2, traces 1 and 2). The pH gradient was readily dissipated by addition of 5 μM CCCP. No proton pumping

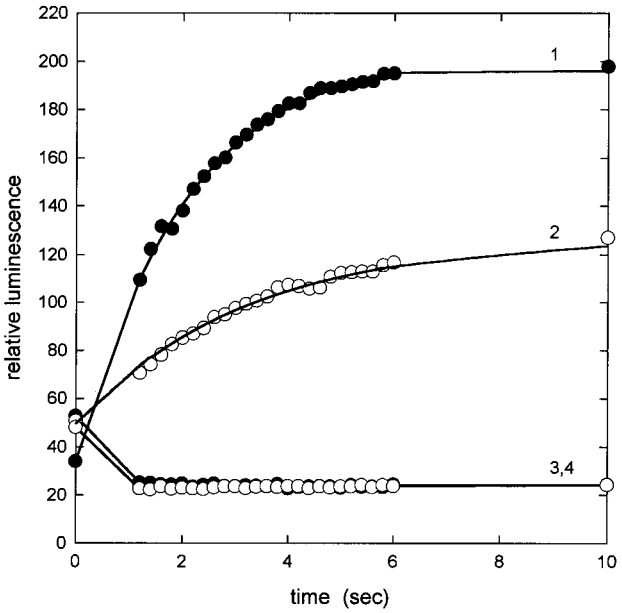

FIGURE 3: Properties of wild-type and βY331W mutant purified F_1F_o. ATP synthesis in proteoliposomes. F_1F_o was reconstituted into PC/PG liposomes and ATP synthesis was monitored using luciferin/luciferase as described in Experimental Procedures. At time zero, F_1F_o proteoliposomes in buffer containing 20 mM succinate, pH 4.7, 0.6 mM KCl, 2.5 mM $MgCl_2$, 5 mM NaH_2PO_4, 0.2 mM ADP, and 8 μM valinomycin were rapidly injected into buffer containing 200 mM Tricine, pH 8.8, 50 mM KCl, 2.5 mM $MgCl_2$, 5 mM NaH_2PO_4, 0.2 mM ADP, and 1.6 mg/mL of luciferin/luciferase reagent. After an experimental dead-time of one second, data points were registered by the luminometer every 0.2 s. Traces 1 and 3, wild-type F_1F_o; traces 2 and 4, βY331W F_1F_o; traces 1 and 2, no DCCD; traces 3 and 4, F_1F_o proteoliposomes were incubated in 150 μM DCCD for 20 min at room temperature prior to addition to succinate-containing buffer. Symbols represent data points, the lines are fits to the data points (see Results).

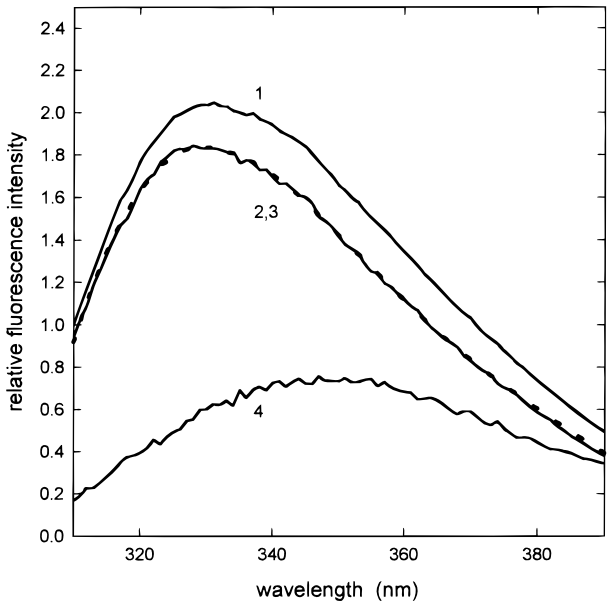

FIGURE 4: Fluorescence emission spectra of purified βY331W F_1F_o. The protein concentration in the cuvette was 20 nM, and all spectra are corrected (λ_{exc} = 295 nm). For other conditions, see Experimental Procedures. Curve 1, βY331W F_1F_o in absence of nucleotide; curve 2, βY331W F_1F_o after addition of 1 mM MgATP; curve 3, wild-type F_1F_o in absence or presence of 1 mM MgATP; curve 4, difference spectrum of mutant versus wild-type F_1F_o (enhanced by a factor of 3).

was observed when F_1F_o samples were preincubated in 150 μM DCCD prior to reconstitution (Figure 2, traces 3 and 4). Proton pumping was also abolished when proteoliposomes were preincubated in 150 μM DCCD, or DCCD was added directly to pumping proteoliposomes, and venturicidin also proved to be a potent inhibitor of ATP-driven proton transport in the reconstituted proteoliposomes (data not shown). These results establish the functional integrity of the βY331W mutant F_1F_o preparation.

Proteoliposomes containing wild-type or βY331W F_1F_o could be stripped of the F_1 sector using KSCN (*34*). Without reconstitution with F_1 these proteoliposomes showed no ATP-driven proton pumping, but upon addition of isolated wild-type or βY331W F_1, normal pumping rates were measured. Cross-reconstitution experiments (mutant F_1 with wild-type F_o and vice versa) gave similar results.

ATP Synthesis by Purified F_1F_o in Reconstituted Proteoliposomes. To measure ATP synthesis, wild-type and βY331W F_1F_o were reconstituted into preformed PC/PG (80/20) liposomes as described in Experimental Procedures. Proteoliposomes were energized by a transmembrane acid/base transition with an auxiliary K^+/valinomycin diffusion potential, and ATP synthesis was monitored by luciferin/luciferase in a luminometer. The results are shown in Figure 3. Between injection and start of monitoring, a 1 s time-lapse occurred. ATP synthesis was sustained for about 6 s (Figure 3, traces 1 and 2). Each experiment was calibrated after completed reaction by adding 100 pmol of ATP, to which the system responded instantaneously. When proteoliposomes were pretreated with DCCD (150 μM) no ATP synthesis occurred (Figure 3, traces 3 and 4). Pretreatment of proteoliposomes with CCCP or omission of valinomycin also abolished ATP synthesis (data not shown). Under such "no synthesis" conditions an initial drop of the luminescence was registered for all samples tested, which was due to optical and/or dilution effects after injection of the sample (Figure 3). By fitting the data points to an exponential function, the initial ATP synthesis rate for wild-type F_1F_o was calculated to be 2.89 U/mg (26 s^{-1}), in good agreement with published data (*27*). For βY331W mutant F_1F_o, a rate of 0.74 U/mg (6.6 s^{-1}) was determined. These results confirm the functional integrity of the βY331W F_1F_o preparation.

Fluorescence Properties of Purified βY331W Mutant F_1F_o. Figure 4 shows the corrected tryptophan fluorescence emission spectra of βY331W F_1F_o (trace 1) and wild-type (trace 3). Wild-type contains 18 Trp residues, βY331W mutant contains 21 Trp, accounting for the higher signal from the mutant. The spectra of wild-type and βY331W mutant F_1F_o show maxima at 327 and 333 nm, respectively. In comparison to the equivalent spectra for isolated F_1 (*18*), the maxima in the F_1F_o spectra are slightly blue-shifted, probably due to the hydrophobic milieu of the 9 Trp residues present in the F_o part of the enzyme. The difference spectrum between mutant and wild-type F_1F_o (Figure 4, trace 4, enhanced 3-fold) shows a maximum at about 350 nm, reflecting the hydrophilic environment for the introduced β-331 Trp residues in the (empty) catalytic sites (*3*). The fluorescence signal of the three introduced β-331-Trp residues was large, consistent with previous work on isolated F_1 (*18*). Upon addition of saturating amounts of nucleotide the fluorescence of the three introduced tryptophans was

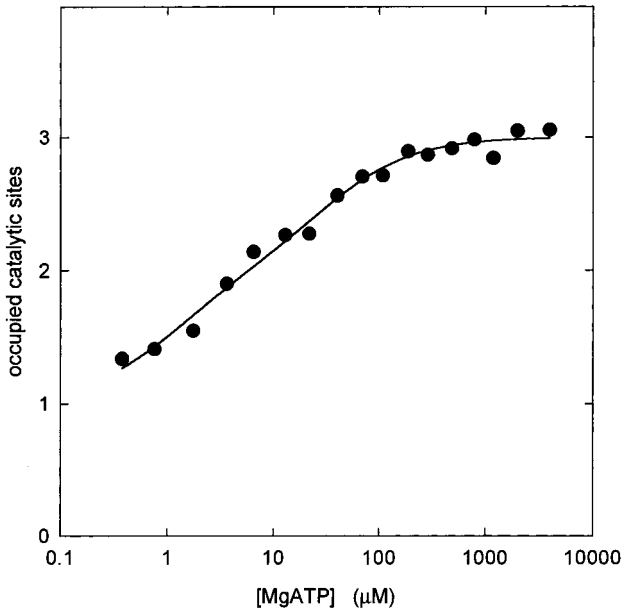

FIGURE 5: MgATP binding to catalytic sites of purified βY331W F_1F_o. Quenching of fluorescence on addition of MgATP was measured as described in Experimental Procedures. Symbols represent data points; the line is a computer-generated fit assuming a model with three different binding sites (*18*, *20*). The equation used was eq 1 from (*30*).

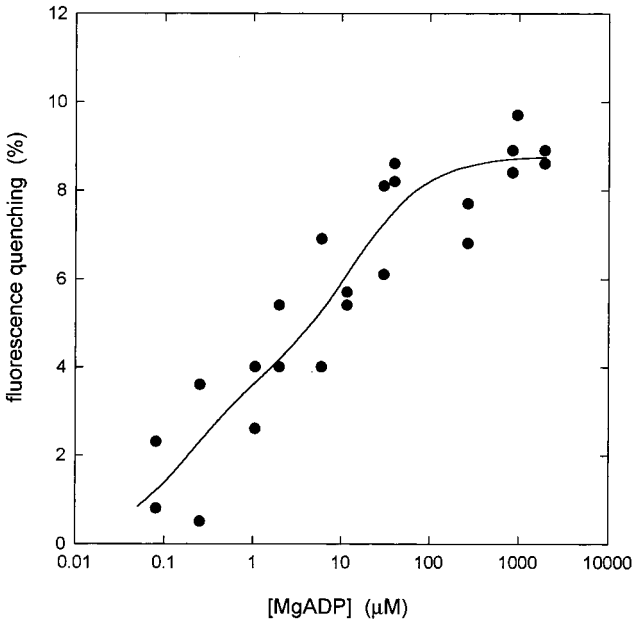

FIGURE 6: MgADP binding to catalytic sites of purified βY331W F_1F_o. Quenching of fluorescence on addition of MgADP was measured as described in Experimental Procedures. Symbols represent data points. The line is a computer-generated fit assuming a model with two classes of binding site (*18*). For calculations, eq 2 from (*30*) was used.

completely quenched (Figure 4, trace 2). The quenching of the fluorescence provided an excellent probe for characterization of binding of nucleotides to the catalytic sites in purified F_1F_o.

Nucleotide Binding to Purified βY331W Mutant F_1F_o. Figure 5 shows the titration curve for MgATP binding to βY331W F_1F_o. Dissociation constants were determined by fitting theoretical binding curves to the experimental data by nonlinear regression analysis. A model with three independent binding sites per enzyme molecule provided an optimal fit for binding of MgATP to the βY331W enzyme. The calculated dissociation constants were $\leq$50 nM for K_{d1}, 1.1 μM for K_{d2}, and 30 μM for K_{d3}. These values may be compared with corresponding values for βY331W F_1 of $\leq$50 nM, 0.5 μM, and 25 μM (*20*). The presence of 5 mM P_i, added to F_1F_o before addition of MgATP, had no influence on the binding curve in Figure 5 (data not shown), indicating that there was no competition between P_i and MgATP at the catalytic sites.

MgADP binding to F_1F_o is displayed in Figure 6. The line represents a fit to a model assuming two classes of binding sites which was adequate to describe the measured data. Calculated K_d values were 0.18 μM for K_{d1} and 13 μM for K_{d2}, with 1.1 binding sites of class one and 1.4 binding sites of class two. Corresponding values determined previously for βY331W F_1 were $K_{d1} = 0.14$ μM and $K_{d2} =$ 20 μM (*18*).

MgAMP (1 mM) had no significant effect on βY331W F_1F_o fluorescence.

Role of Mg^{2+} in Inducing Catalytic Site Asymmetry. Figure 5 has shown that the catalytic sites in F_1F_o are markedly asymmetric in their binding behavior toward MgATP. To determine whether binding cooperativity was dependent on the presence of magnesium, the enzyme was titrated with free ATP in the presence of EDTA. The resulting curve is shown in Figure 7 (solid circles). All three

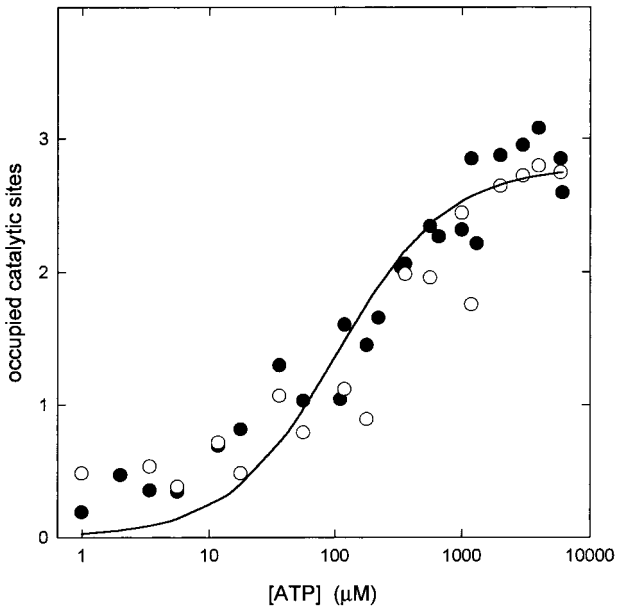

FIGURE 7: ATP binding to catalytic sites of purified βY331W F_1F_o in absence of Mg^{2+}. Quenching of fluorescence on addition of ATP was measured as described in Experimental Procedures. Experiments were carried out in the absence of magnesium and in the presence of 0.5 mM EDTA. Symbols represent data points: ●, absence of P_i; ○, 5 mM P_i present before addition of ATP. The line is a computer-generated fit to the solid symbols assuming a model with one class of binding site. The equation used was eq 3 from (*30*).

sites became saturated with ATP. A computer-generated fit assuming a model with one class of binding site gave a reasonable fit, from which a K_d of 105 μM at each of the three sites could be calculated. For F_1 a corresponding K_d of 71 μM has been determined previously (*20*). However, applying models for two classes of binding sites or three independent binding sites to the data of Figure 7 gave a better

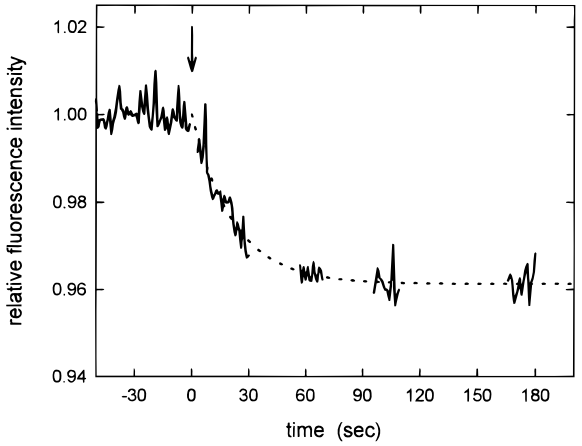

FIGURE 8: The association rate constant for binding of MgATP to purified βY331W F_1F_o. MgATP (80 nM) was added to F_1F_o (20 nM) in a rapidly stirred cuvette at time zero (arrow). The fluorescence was followed by opening the excitation shutter for short intervals and collecting data, then closing it to prevent photobleaching. The line is a fit to the data points. See Results for further details.

fit, with in both cases a calculated $K_{d1} = 5\ \mu$M and $K_{d2,3} = 300\ \mu$M. Previous work with isolated F_1 had not indicated such binding asymmetry with ATP. Therefore this may represent a difference between F_1F_o and F_1. However, a possibility which cannot be discounted is that F_1F_o binds Mg^{2+} ions sufficiently tightly such that EDTA could not extract Mg^{2+} from binding sites (F_1F_o is purified in buffers containing Mg^{2+}). Thus, upon addition of ATP, a fraction of the nucleotide would be bound as MgATP, resulting in artificially increased apparent affinity at low ATP concentration. In any case, it is clear that in F_1F_o, as in F_1, the presence of magnesium brings about an enormous increase in binding affinity of catalytic sites 1 and 2 for ATP.

The open circles in Figure 7 are the results obtained when P_i (5 mM) was added (in the presence of EDTA) before addition of ATP. Again it is seen that there was no binding of P_i to the catalytic sites.

Determination of the Association Rate Constant for MgATP. To measure the association rate constant for MgATP it was necessary to work at low nucleotide concentrations. In the experiments, F_1F_o was added at a concentration of 20 nM and MgATP at 80 nM. Under these conditions it is expected that, primarily, binding to the first catalytic site is being measured. Figure 8 shows the time course of the fluorescence observed upon addition of MgATP. Quenching was essentially complete in ~60 s. To determine the association rate constant a fit to the data points was calculated, represented by the dotted line in Figure 8. The derived rate constant is $5.7 \times 10^5\ M^{-1}\ s^{-1}$.

Preliminary experiments showed that the enzyme was susceptible to photobleaching in the absence or presence of low concentration of nucleotide. To avoid photobleaching the excitation shutter remained closed between periods of data collection, which is the reason for the discontinuity of the data points in Figure 8. A slow decrease of the fluorescence signal occurring over a time course of several minutes was seen previously in studies of isolated F_1 (*18*), and subsequent experiments have shown that photobleaching was the likely cause in that work also.

Correlation of ATP Hydrolysis Activity and Catalytic Site Occupancy. ATPase activity and fluorescence quenching were measured in parallel, using identical experimental conditions. Enzymatic activity was determined from the amount of P_i liberated 60 s after addition of MgATP, the fluorescence quench was also registered 60 s after addition of the nucleotide. Both curves are shown in Figure 9, where occupancy of catalytic sites (squares) and ATPase activity (circles) are plotted versus MgATP concentration. To calculate K_M(MgATP), a theoretical curve was fitted to the experimental data, assuming a model with a single K_M. The achieved fit described the results satisfactorily, and a K_M-(MgATP) of 24 μM was obtained. As shown above, the K_d values for binding of MgATP are $\leq$50 nM (K_{d1}), 1.1 μM (K_{d2}), and 30 μM (K_{d3}). Clearly K_{d3} correlates well with K_M(MgATP), showing that in F_1F_o all three catalytic sites must be filled to reach V_{max} rates of ATP hydrolysis.

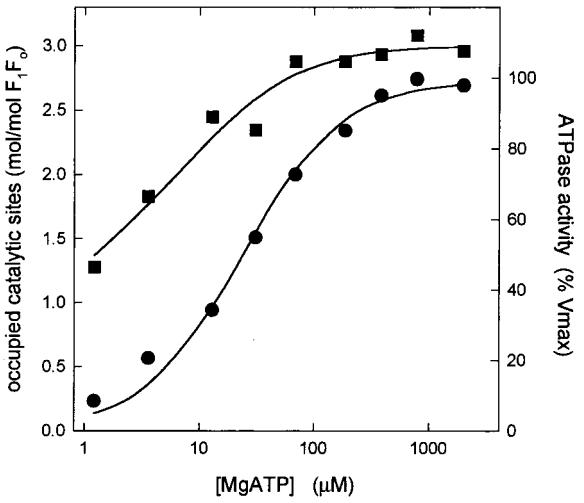

FIGURE 9: Catalytic site occupancy and ATPase activity in purified βY331W F_1F_o. ATPase activity and fluorescence quenching were assayed as a function of MgATP concentration under identical conditions (50 mM Tris/H_2SO_4, pH 8.0, 23 °C, ATP/$MgSO_4$ ratio of 2.5/1, protein concentration 15 nM). ■, MgATP binding assayed by fluorescence (left axis); ●, ATPase activity assayed by P_i release (right axis).

In Figure 10, ATPase activity is plotted against the fraction of catalytic sites occupied in the entire enzyme molecule population, using the data from Figure 9. The filled circles represent ATPase activities at different fractional values of catalytic site occupancy. It is immediately evident from this Figure that V_{max} was achieved only when all three catalytic sites in every enzyme molecule were filled by nucleotide. The dotted line is the result of a simulation based on the assumption that V_{max} for ATPase activity is achieved only when all three catalytic sites are filled with nucleotide (i.e., an enzyme molecule with only two sites filled has zero activity). The dashed line represents a fit assuming that maximal ATP hydrolysis is achieved by enzyme molecules with either two or three catalytic sites filled. The solid line in Figure 10 is a computer-generated fit to the actual data points. This indicated that enzyme molecules with only two of the three catalytic sites filled achieved an ATPase activity equal to 4.7% of V_{max}.

DISCUSSION

The goal of this work was to characterize the nucleotide binding properties of the three catalytic sites of purified entire F_1F_o-ATP synthase from *E. coli* and to establish the

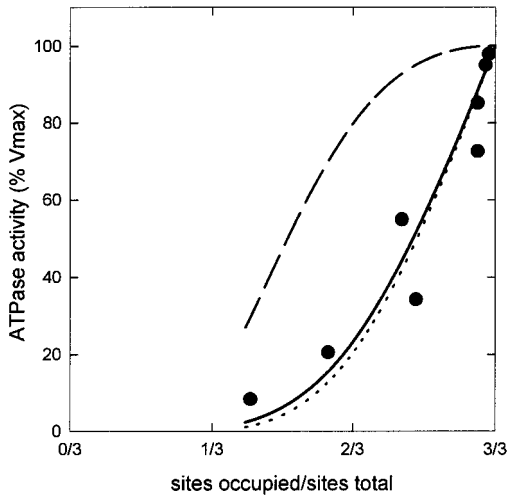

FIGURE 10: Correlation of ATPase activity with catalytic site occupancy. The solid circles are data for measured ATPase activity plotted versus measured fraction of catalytic sites occupied (from Figure 9). The dotted line is the theoretical curve expected for the situation if only enzyme molecules with three catalytic sites filled are able to hydrolyze ATP; i.e., the ATPase activity of an enzyme molecule with only two sites filled is negligible (calculated as in ref *18*). The dashed line describes the case where V_{max} ATPase activity is achieved by enzyme molecules with either two or three catalytic sites filled. The solid line is a fit to the measured data points, which indicates that the ATPase activity of an enzyme molecule with only two catalytic sites filled is equal to 4.7% of V_{max}.

relationship between occupancy of catalytic sites and ATP hydrolytic activity. Nucleotide binding parameters were obtained using the fluorescence signal of residue β-Trp-331, in the βY331W mutant enzyme. Residue β-331 is known from X-ray structure analysis to make extensive contact with the adenine ring of bound nucleotide substrate in the catalytic sites (*3*, *30*), resulting in complete quenching of the large fluorescence signal (*18*).

Since very little work has been published previously using purified mutant F_1F_o from any source, our first concern was to obtain purified *E. coli* mutant βY331W F_1F_o and to establish its structural and functional integrity, The method of Moriyama et al. (*23*) was found to be effective for purification. The data in Figures 1−3 established that the purified mutant F_1F_o had normal eight-subunit composition with high purity, showing normal ATP-driven proton-pumping activity, and high rates of ATP synthesis activity.

The tryptophan fluorescence spectrum of the βY331W mutant F_1F_o was enhanced over that of wild-type by about 15%, and on addition of physiological concentration (1 mM) of MgATP the fluorescence signal was quenched down to that of wild-type (Figure 4). This demonstrated that the fluorescence signal of the β-Trp-331 residues could be used to monitor nucleotide binding in the mutant F_1F_o, and indeed that at physiological concentrations of MgATP substrate, all three catalytic sites became filled.

Studies of binding of the natural substrates MgATP and MgADP were then carried out, revealing strong cooperativity of binding and asymmetry of the three catalytic sites. For MgATP three different K_d values were found ($\leq$50 nM, 1.1 μM, and 30 μM); for MgADP two different K_d values were seen (0.18 and 13 μM) with one site of higher and two sites of lower affinity. The data establish that purified F_1F_o shows virtually the same substrate binding behavior as is seen in isolated F_1 (*18*−*22*). This is important because it demonstrates that the additional subunits present in F_1F_o (*a*, *b*, *c*, and full stoichiometric levels of δ and ϵ) have no effect per se on catalytic site binding properties, and that under in vivo conditions the three catalytic sites of F_1F_o would be filled by cellular adenine nucleotides.

No evidence for P_i binding by purified F_1F_o was seen at physiological concentration of 5 mM P_i. This demonstrates that during ATP synthesis in cells, spontaneous binding of P_i to the catalytic sites cannot occur unless there is *prior* input of energy from the proton gradient in the form of conformational tension in the catalytic site which radically changes the binding affinity for P_i. A model for ATP synthesis encompassing this concept has been developed (*35*, *36*). Models for ATP synthesis that envisage spontaneous P_i binding to the catalytic sites without prior energy input must be incorrect (e.g., ref 37).

Mg^{2+} was found to be a critical determinant of catalytic site nucleotide-binding cooperativity and asymmetry. In the presence of EDTA, purified F_1F_o bound ATP at all three sites (Figure 7), but with very much reduced affinity at sites one and two. We could not conclude that asymmetry was totally abolished in absence of Mg^{2+} (see Results), but certainly it was very much reduced, supporting our earlier conclusion that Mg^{2+} is the crucial determinant of catalytic site asymmetry (*20*−*22*). Kaibara et al. (*38*) have recently stated that the γ-subunit is also critical for generation of the high-affinity catalytic site, although it may be noted that the $\alpha_3\beta_3$ complex, lacking γ, showed both high-affinity binding and hydrolysis of the analogue MgTNP-ATP (Figure 4B of ref 38). Since the γ-subunit does not make contact with catalytic-site bound nucleotide directly (*3*), its effects must be indirect, mediated through groups that directly ligand to the nucleotide.

On addition of MgATP to purified βY331W F_1F_o, the fluorescence response was shown to be very rapid, yielding an association constant of 5.7×10^5 M^{-1} s^{-1}. As noted in Results, this value would apply primarily to binding at site one, and is the same as that found in isolated F_1 using "unisite" techniques (*39*). From ATPase assays conducted under "multisite" conditions, k_{cat}/K_M(MgATP) was found to be around 10^6 M^{-1} s^{-1} (above). Therefore we may conclude that in F_1F_o the association constants for MgATP binding at all three catalytic sites are similar.

In Figures 9 and 10 we investigated the relationship between ATPase activity and the degree of occupancy of catalytic sites in purified F_1F_o. The unambiguous conclusion is that only enzyme molecules with all three catalytic sites filled display V_{max} activity. It was calculated that a purified F_1F_o molecule with only two catalytic sites filled displays 4.7% of V_{max} activity. Similar results were seen previously in isolated F_1 (*18*, *19*) where the ATPase activity of an enzyme molecule with two sites filled was calculated to amount to $\leq$2% of V_{max}. As comparison of the solid and dotted lines in Figure 10 exemplifies, not too much significance should be attached to the absolute values of these numbers. It is germane, however, to consider whether such activities are physiologically relevant. Studies on numerous *E. coli* mutants in our laboratory and in others have established that when the catalytic activity of ATP synthase is reduced below 10% of wild-type V_{max} by mutation, growth

of cells by oxidative phosphorylation on nonfermentable substrates is not possible. Since the data in Figure 10 may be interpreted confidently as showing that the catalytic activity of a molecule of F_1F_o with only two catalytic sites occupied by substrate is less than 10% of V_{max}, then it follows that only the enzyme species with all three sites occupied can achieve physiological rates of catalysis.

This has important consequences. Some models of ATP synthase mechanism postulate that there is always one catalytic site out of the three that is unoccupied during the catalytic cycle. Such models must be incorrect because at no stage do they include an enzyme species capable of physiological rate of catalysis. Furthermore, it has also been claimed that during catalysis, substrate binding and product release occur simultaneously. Such models are also necessarily incorrect. Since the physiologically relevant, catalytically competent enzyme species is the one with all three catalytic sites occupied by nucleotide, it must be that product dissociates first to reveal an open, available catalytic site, before a molecule of substrate can subsequently bind from the medium.

In summary, we have purified F_1F_o from *E. coli* βY331W mutant and established nucleotide binding parameters of F_1F_o catalytic sites for the first time. The results demonstrate strong binding cooperativity and asymmetry of catalytic sites, dependent upon the presence of Mg^{2+}. At cellular adenine nucleotide concentration, all three catalytic sites were filled, but P_i, at cellular concentration, did not bind to catalytic sites. Nucleotide binding was rapid. The results unambiguously establish that all three catalytic site must be filled for the physiological rate of catalysis to be achieved, and thereby set important limitations on postulated mechanisms. Perhaps most importantly, it now appears feasible to use the tryptophan fluorescence of purified F_1F_o to study modulations of nucleotide binding parameters during ATP-driven proton-pumping and ATP synthesis.

REFERENCES

1. Nakamoto, R. K. (1996) *J. Membr. Biol. 151*, 101−111.
2. Weber, J., and Senior, A. E. (1997) *Biochim. Biophys. Acta 1319*, 19−58.
3. Abrahams, J. P., Leslie, A. G. W., Lutter, R., and Walker, J. E. (1994) *Nature 370*, 621−628.
4. Van Raaij, M. J., Abrahams, J. P., Leslie, A. G. W., and Walker, J. E. (1996) *Proc. Natl. Acad. Sci. U.S.A. 93*, 6913−6917.
5. Abrahams, J. P., Buchanan, S. K., Van Raaij, M. J., Fearnley, I. M., Leslie, A. G. W., and Walker, J. E. (1996) *Proc. Natl. Acad. Sci. U.S.A. 93*, 9420−9424.
6. Shirakihara, Y., Leslie, A. G. W., Abrahams, J. P., Walker, J. E., Ueda, T., Sekimoto, Y., Kambara, M., Saika, K., Kagawa, Y., and Yoshida, M. (1997) *Structure 5*, 825−836.
7. Uhlin, U., Cox, G. B., and Guss, J. M. (1997) *Structure 5*, 1219−1230.
8. Wilkens, S., Dahlquist, F. W., McIntosh, L. P., Donaldson, L. W., and Capaldi, R. A. (1995) *Nat. Struct. Biol. 2*, 961−967.
9. Wilkens, S., Dunn, S. D., Chandler, J., Dahlquist, F. W., and Capaldi, R. A. (1997) *Nat. Struct.Biol. 3*, 198−201.
10. Fillingame, R. H., Girvin, M. E., and Zhang, Y. (1995) *Biochem. Soc. Trans. 23*, 760−766.
11. Noji, H., Yasuda, R., Yoshida, M., and Kinosita, K., Jr. (1997) *Nature 386*, 299−302.
12. Yasuda, R., Noji, H., Kinosita, K., Jr., Motojima, F., and Yoshida, M. (1997) *J. Bioenerg. Biomembr. 29*, 207−209.
13. Cross, R. L. (1981) *Ann. Rev. Biochem. 50*, 681−714.
14. Weber, J., Wilke-Mounts, S., Grell, E., and Senior, A. E. (1994) *J. Biol. Chem. 269*, 11261−11268.
15. Weber, J., and Senior, A. E. (1995) *J. Biol. Chem. 270*, 12653−12658.
16. Weber, J., Bowman, C., Wilke-Mounts, S., and Senior, A. E. (1995) *J. Biol. Chem. 270*, 21045−21049.
17. Weber, J., and Senior, A. E. (1997) *FEBS Lett. 412*, 169−172.
18. Weber, J., Wilke-Mounts, S., Lee, R. S. F., Grell, E., and Senior, A. E. (1993) *J. Biol. Chem. 268*, 20126−20133.
19. Weber, J., Bowman, C., and Senior, A. E. (1996) *J. Biol. Chem. 271*, 18711−18718.
20. Weber, J., Wilke-Mounts, S., and Senior, A. E. (1994) *J. Biol. Chem. 269*, 20462−20467.
21. Weber, J., and Senior, A. E. (1996) *J. Biol. Chem. 271*, 3474−3477.
22. Weber, J., Hammond, S. T., Wilke-Mounts, S., and Senior, A. E. (1998) *Biochemistry 37*, 608−614.
23. Moriyama, Y., Iwamoto, A., Hanada, H., Maeda, M., and Futai, M. (1991) *J. Biol. Chem. 266*, 22141−22146.
24. Rao, R., Al-Shawi, M. K., and Senior, A. E. (1988) *J. Biol. Chem. 263*, 5569−5573.
25. Kagawa, Y., and Racker, E. (1971) *J. Biol. Chem. 246*, 5477−5487.
26. Richard, P., Rigaud, J. L., and Gräber, P. (1990) *Eur. J. Biochem. 193*, 921−925.
27. Fischer, S., Etzold, C., Turina, P., Deckers-Hebestreit, G., Altendorf, K., and Gräber, P. (1994) *Eur. J. Biochem. 225*, 167−172.
28. Taussky, H. H., and Shorr, E. (1953) *J. Biol. Chem. 202*, 675−685.
29. van Veldhoven, P. P., and Mannaerts, G. P. (1987) *Anal. Biochem. 161*, 45−48.
30. Löbau, S., Weber, J., Wilke-Mounts, S., and Senior, A. E. (1997) *J. Biol. Chem. 272*, 3648−3656.
31. Pecoraro, V. L., Hermes, J. D., and Cleland, W. W. (1984) *Biochemistry 23*, 5262−5271.
32. Bradford, M. M. (1976) *Anal. Biochem. 72*, 248−254.
33. Laemmli, U. K. (1970) *Nature 227*, 680−685.
34. Perlin, D. S., Latchney, L. R., Wise, J. G., and Senior, A. E. (1984) *Biochemistry 23*, 4998−5003.
35. Al-Shawi, M. K., Parsonage, D., and Senior, A. E. (1990) *J. Biol. Chem. 265*, 4402−4410.
36. Al-Shawi, M. K., Ketchum, C. J., and Nakamoto, R. K. (1997) *Biochemistry 36*, 12961−12969.
37. Cross, R. L., and Duncan, T. M. (1996) *J. Bioenerg. Biomembr. 28*, 403−408.
38. Kaibara, C., Matsui, T., Hisabori, T., and Yoshida, M. (1996) *J. Biol. Chem. 271*, 2433−2438.
39. Senior, A. E., Lee, R. S−F., Al-Shawi, M. K., and Weber, J. (1992) *Arch. Biochem. Biophys. 297*, 340−344.

BI9807153